E|DPC-2016

Electric Drives Production
Conference 2016

6th International Conference

Electric Drives Production

November 30th – December 1st, 2016
Nuremberg, Germany

Proceedings

MARSILLI

Bühler Motor

ZIEHL-ABEGG

TEMPEL

AMA Verband für Sensorik + Messtechnik

ECPE

EMCW

UK Magnetic Society

Nürnberg

BEM eMobilität

antriebstechnik

Automation Valley Nord-Bayern

Bayern Innovativ

MHI Wissenschaftliche Gesellschaft Montage Handhabung Industrierobotik

BÜHLER MOTOR MECHATRONIC AWARD 2016

cluster mechatronik & automation

ETG Power Engineering Society within VDE

VDE

FAPS

FVA Forschungsvereinigung Antriebstechnik e.V.

metropolregion nürnberg SEE IT. FEEL IT. STAY.

pels IEEE Power Electronics Society Powering a Sustainable Future

IHK Industrie- und Handelskammer Nürnberg für Mittelfranken

conf Make your conference easy

IEEE

VDMA Antriebstechnik

Green Factory BAVARIA

E|Home-Center Bavarian Technology Center for Domestic Living

E|Drive-Center Bayerisches Technologiezentrum für elektrische Antriebstechnik

Methods for hysteresis losses determinations at non-standard ring core geometries equivalent to Epstein measurements

Abdullah Kahveci, Philipp Szary, Florian Herget
Department of Application Engineering
thyssenkrupp Steel Europe AG
Bochum, Germany
abdullah.kahveci@thyssenkrupp.com

Aryanti Kusuma Putri, Kay Hameyer
Institute of Electrical Machines
RWTH Aachen University
Aachen, Germany

***Abstract*—The iron losses in electrical machines differ significantly from those of measurements using the standardized measurement method, i.e. by use of an Epstein frame. In order to obtain a better approximation of the losses in an electrical machine, several toroidal geometries were examined more closely. In the first step, according to the standardized method, a ring-geometry was chosen, which corresponds to the magnetic path length of the Epstein frame. Starting from this reference ring and by gradual reduction of the diameter, further ring cores were measured. Within this framework, different methods were used, in which e.g. the influence of axial height, length of the cutting edge relative to the area or the ratio of outer and inner diameter was investigated. In addition to the measurements, numerical calculations were performed. Here, the focus lies on the exploration of the field density distribution over the ring width with respect to the various methods. Taking into account for those processing effects with the highest impact, the smallest geometries of each method and the largest ring, acting as a reference, were studied in detail. The investigations on the toroidal cores of the methods were carried out at a frequency of 400 Hz and a target minimum polarization of 1.0 T. As a final outcome, a recalculation of an existing machine with the new parameters of a selected ring nucleus was done.**

Keywords— magnetic properties, ring cores

I. INTRODUCTION

The magnetic circuit of an electrical machine is constructed of rotor and stator lamination stacks, which are built from non-grain-oriented electrical steel. For this purpose, the electrical steel undergoes an extensive manufacturing process, which could deteriorate its magnetic properties. This would lead to e.g. increase of hysteresis losses [1].

The characterization of electrical steel is performed according to the norm IEC 60404-2 at a frequency of f = 50 Hz and a polarization of J = 1.5 T using rectangle samples with a side length between 280 mm and 320 mm. These samples, the so called Epstein strips, are nested in an Epstein frame, which is shown in Fig. 1. The primary coils of the Epstein frame are fed with sinusoidal current, which induces an alternating field in the Epstein strips. The hysteresis losses are measured under this condition [2].

The magnetic field distribution in stator and rotor of an electrical machine differs from the distribution in Epstein strips. The field in an electrical machine is a rotating field, which is produced from its winding configuration fed by a 3-phase-current. In case of a permanent magnet synchronous machine (PMSM), the rotating field superposes with the DC field of the magnets. The sum of the magnetic fields in the laminated cores are hereby non-sinusoidal. As a result of the superposition of magnetic fields, higher field harmonics are induced in the laminated cores. This complicates the calculation of the iron losses. Furthermore, due to deviation caused by the production of the electrical steel, the properties of the electrical steel are varied in terms of material thickness, grain size distribution and magnetic anisotropy. An a priori calculation of the iron losses of the electrical machines based solely on measurements with Epstein procedure is only possible under certain conditions. Even an approximation of the losses is sometimes inaccurate due to the non-linear characteristic of the material properties. As an alternative to the Epstein strips and an approximation of the stator, a ring core with a toroidal winding (toroid inductor) can be used for the measurements of the magnetic properties. A study of the core geometry based on the norm IEC 60404-6 is conducted. According to [3] the maximum ratio between outer and inner diameter of the core d_o / d_i should not be larger than 1.4, empirically the suggested value is $d_o / d_i < 1.25$.

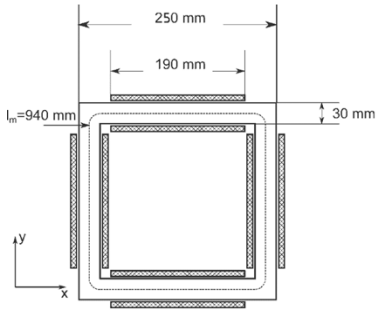

Fig. 1: Epstein frame [2].

II. Experimental Study

For the experimental study, a reference ring core with magnetic path length similar to the Epstein frame, i.e. l_m = 940 mm, is utilized (Epstein ring). The used core material is the electrical steel grade 280-30AP (thickness d = 0.30 mm). In total, 44 Epstein strips are used for the measurement with the Epstein procedure. Divided by the sides of the rectangle, the axial height of the setups is h = 3.30 mm. The Epstein ring hast an identical height. The outer and inner diameter of the ring core are d_o = 330 mm and d_i = 270 mm. The magnetic path length can be calculated with [4]:

$$l_{m,Log} = \frac{d_o - d_i}{\ln\left(\frac{d_o}{d_i}\right)}\pi = \frac{330\ mm - 270\ mm}{\ln\left(\frac{330\ mm}{270\ mm}\right)}\pi = 939\ mm\ . \quad (1)$$

To study the influence of the ring core geometry and the manufacturing process, in this case the cutting edge effect, on the hysteresis losses, the diameters of the rings are successively decreased. Three methods to investigate these effects are analyzed.

In the first method, the width of the ring core in the radial direction is kept constant at 30 mm and the height is kept constant at 3.30 mm. The reduction of the diameter is shown in Fig. 2.

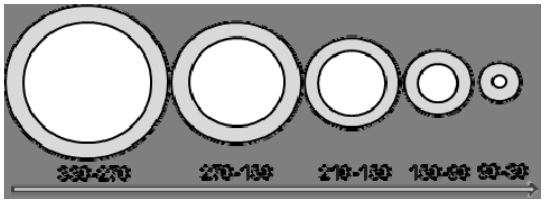

Fig. 2: Reduction of the ring core diameters at a constant width of 30 mm in the radial direction (method 1).

In the second method, shown in Fig. 3, the width of the ring core in the radial direction is reduced in addition to reduction of the diameters. The area, which is inflicted by the cutting process, increases with smaller ring diameter. The height of the ring core is kept constant at 3.30 mm.

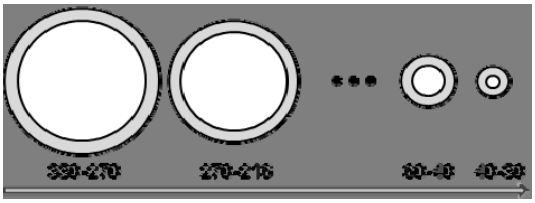

Fig. 3: Reduction of the diameter and the thickness of the ring cores in the radial direction 330-270, 270-216, 216-168, 168-126, 126-90, 90-60, 60-40, 40-30 (method 2).

The last method is similar with the first method, except that the height of the ring core is increased with smaller ring diameters. With this method, the mass of the ring core is kept constant. The increase of the axial height is shown in Fig. 4.

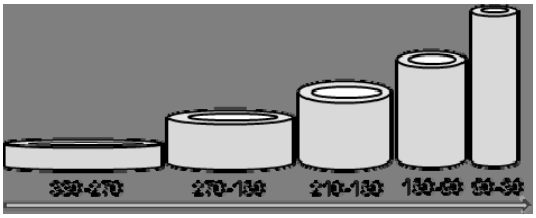

Fig. 4: Reduction of the ring core diameters and increase of the ring core height (method 3).

The influences of the manufacturing process increase with higher ratio of cutting edge length to area (L_{cut}/ A) and thereby lead to deterioration of the magnetic properties [1]. For this reason, the reference ring and the ring cores with smallest diameters are examined in detail (Tab. 1 and Fig. 5). The ring cores are measured with identical magnetic polarization J and frequency f. Due to the difference in the magnetic path length, the number of windings for each ring has to be adjusted. The ratio of the outer to inner ring core diameter

$$\frac{d_o}{d_i} \quad (2)$$

and the ratio of the cutting edge length to the area

$$\frac{L_{cut}}{A} = \frac{L_{u,a} + L_{u,i}}{A_{ring}} \quad (3)$$

of the reference ring and the examined ring cores are different (Tab. 1).

Tab. 1: The examined ring cores.

Core Type	d_o/ mm	d_i/ mm	b_{ring}/ mm	d_o/d_i	L_{cut}/A / mm^{-1}
Epstein ring 260	330	270	30	1.22	0.067
Ring 90-30 (3.3)	90	30	30	3.00	0.067
Ring 40-30	40	30	5	1.33	0.400

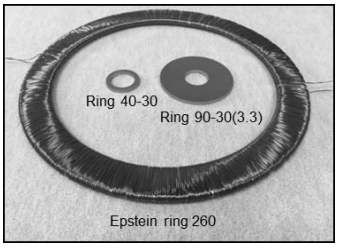

Fig. 5: The examined ring cores.

In Fig. 6, the specific losses of the examined ring cores at 400 Hz as function of the magnetic polarization *J* are shown. The specific losses of the reference ring and the ring 90-30(3.3) of method 1 at 1.5 T are similar, ca. 40 W/kg. The specific losses

of the ring 40-30 of method 2 are much higher, with ca. 59 W/kg at 1.5 T.

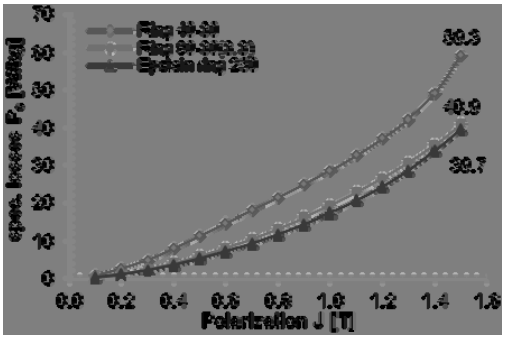

Fig. 6: The specific losses of the examined ring cores at 400 Hz.

To compare the losses of the examined rings to the reference ring, the loss factor is introduced:

$$Loss \quad factor \quad = \frac{P_{S\,(ex.\,ring\,)}}{P_{S\,(Epstein \quad ring\,)}}. \qquad (4)$$

The loss factors of the examined rings are shown in Fig. 7. The loss factor of the ring 90-30(3.3) is slightly higher than that of the reference ring. Its maximum is at 0.1 T with the value of 1.15 and sinks with increasing polarization and reaches its minimum at 1.5 T with a value of 1.03. The ratio of the cutting edge length to the area of the reference ring and the ring 90-30(3.3) of method 1 are identical, i.e. the influences of the manufacturing process on these rings are similar. The ratio of the outer to inner diameter of the reference ring is $d_o / d_i = 1.22$, which is below the required value of 1.4 (IEC 60404-6). On the contrary, the ring 90-30(3.3) has a ratio of $d_o / d_i = 3.00$, which influences the field distribution in the ring core and thus the iron losses. The detailed analysis of the field distribution will be described in the next chapter.

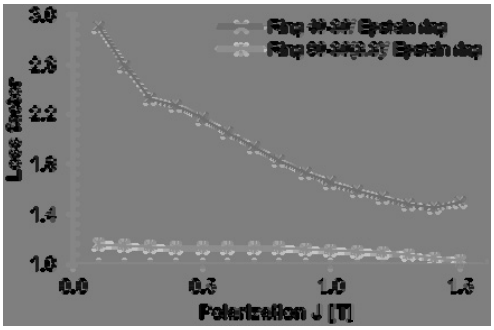

Fig. 7: Loss factor of the examined rings at 400 Hz.

The ring 40-30 of method 2 has a ratio of outer to inner diameter of $d_o / d_i = 1.33$ and satisfies the norm IEC 60404-6. However, the ratio of the cutting edge length to the ring area is 6 times higher than that of the other rings. The loss factor of this ring is also higher than that of the ring of method 1. The maximum loss factor lies at 0.1 T with a value of 2.9. The loss factor decreases with increasing polarization and its minimum lies slightly below 1.5, i.e. 50 % higher than the losses of the reference ring.

The magnetization curves of the examined rings are shown in Fig. 8. The reference ring required the lowest magnetic field strength to reach a polarization up to 1 T. The curve overlapped with the ring 90-30(3.3) of method 1 at 1.1 T. Due to the number of windings and the maximum induced voltage of the test bench, the reference ring could only be measured up to 1.5 T. An approximation of the curve closes in on the magnetization curve of the ring 40-30 of method 2, which is common at saturation points.

The ring 90-30(3.3) of method 1 could reach the polarization value of 1.7 T and requires a low magnetic field strength starting at 1.2 T, when compared to the other rings. The curve isn't draw nearer to the other curves. This can be caused by the high ratio of outer to inner diameter of the ring core. The magnetization characteristic over the width of the ring is affected.

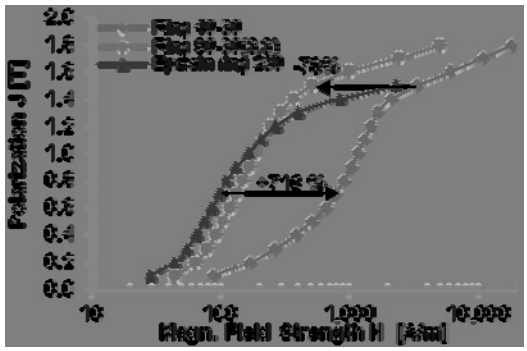

Fig. 8: Magnetization curves of the examined ring cores at 400 Hz.

Due to the higher ratio of the cutting edge length and the ring area, the magnetization curve of the ring 40-30 of method 2 deviates from the curve of the other rings. At a polarization of 0.7 T, the ring 40-30 of method 2 requires 710 % higher magnetic field strength than the reference ring.

In Fig. 9 the hysteresis curves up to a polarization of 0.5 T at 400 Hz of the examined ring cores are shown. The deterioration of the magnetic properties of the ring 40-30 can be recognized through the remarkable shearing of the curve. On the contrary, the curve of the ring 90-30(3.3) lies close to the curve of the reference ring. The coercivity H_c of the reference ring, the ring 90-30(3.3) of method 1 and the ring 40-30 of method 2 are 61 A/m, 70 A/m and 140 A/m, respectively.

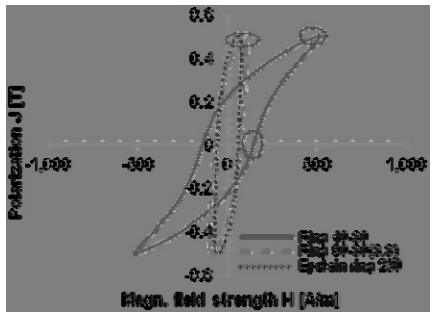

Fig. 9: Hysteresis curves up to J = 0.5 T at 400 Hz of the examined ring cores.

A comparable behavior is found in Fig. 10. Here, the hysteresis curves up to a polarization of 1.5 T at 400 Hz of the examined ring cores are shown.
Similar to Fig. 9, the hysteresis curve of the ring 40-30 of method 2 shears considerably. On the contrary, the curves of the reference ring and the ring 90-30(3.3) possess a comparable behavior without shearing for lower polarization. At higher polarization of about 1.2 T, a strong deviation of both curves is encountered, which is in accordance with Fig. 8. I.e., at polarization levels > 1.2 T the ring 90-30(3.3) requires much smaller field values, whereas the curves of the ring 40-30 and the reference ring already show a saturating behavior. Since all rings are manufactured of the same material and the reference ring and the ring 90-30(3.3) exhibit the same ratio of cutting edge length to area, it is assumed that the ratio of outer to inner diameter d_o / d_i has a significant influence on the magnetization process. In case of the ring 90- 30(3.3), the value is 3 and therewith higher than 1.4, as it is recommended within the norm. In case of the Epstein ring it is d_o / d_i = 1.22. A difference due to mechanical stress from the winding process is excluded since it is comparable for all rings.

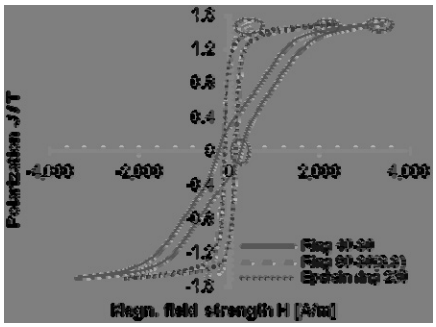

Fig. 10: Hysteresis curves up to J = 1.5 T at 400 Hz of the examined ring cores.

In addition to ring core diameters, the influences of the ring core height are studied. The ring 90-30(3.3) of method 1 will be compared with the ring 90-30(16.5) of method 3. The ring cores are illustrated in Fig. 11. The diameters of both rings are identical. The mass of the ring 90-30(16.5) is 5 times higher than the mass of the ring 90-30(3.3).

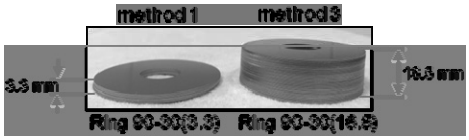

Fig. 11: Ring 90-30 with the height of 3.3 mm (left) and 16.5 mm (right).

The loss factor is calculated as the loss ratio of the ring 90-30(3.3) to the ring 90-30(16.5). The results are presented in Fig. 12. It is shown, that the specific iron losses of both rings are similar. The maximum difference lies below 2 %. The mean value of the difference is 0.5 %.

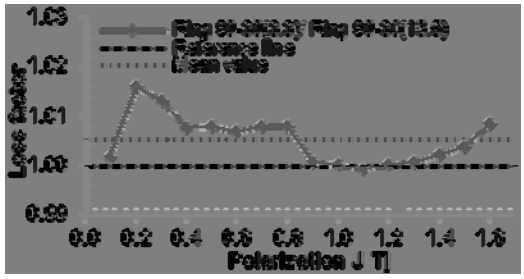

Fig. 12: Loss factor of the examined rings 90-30 with the height 3.3 mm and 16.5 mm at 400 Hz.

The rings 90-30 with height of 3.3 mm and 16.5 mm show a similar characteristic of the magnetization curves. To compare the magnetization curves, the magnetic field strength factor is introduced:

$$Field\quad strength\quad factor\ = \frac{H\,(Ring\ \ 90\ -\ 30\,(3.3))}{H\,(Ring\ \ 90\ -\ 30\,(16.5))}. \qquad (5)$$

The calculated magnetic field strength factor is presented in Fig. 13. In the area with low magnetic polarization, the thinner ring requires higher magnetic field to reach the same value of flux density. E.g., at 0.1 T, the ring 90-30(3.3) needs 15 % higher field strength than the ring 90-30(16.5). The deviation can be traced back to the high material sensitivity in this area. With higher magnetization, the field strength factor decreases. The magnetization curves of both rings overlap at 1.2 T.

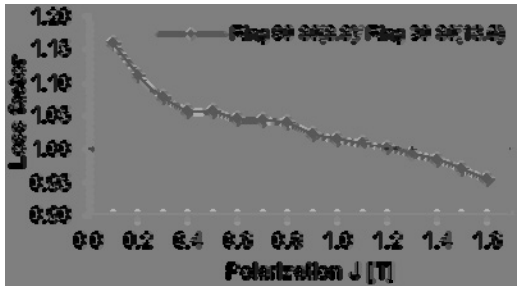

Fig. 13: Magnetic field strength factor of the ring 90-30(3.3) and 90-30(16.5) at 400 Hz.

III. Numerical Examination

The measured ring core geometries are simulated with 2D Finite-Element-Method (FEM) using the pyMOOSE simulation tool. The influences of the ring axial height are taken into account through utilizing the measured magnetization curves as input data. The influences of the manufacturing procedure are neglected. In addition to the iron losses, the field distributions in each ring core are examined. The material properties of the ring cores are described by the measured magnetization curves, which are shown in Fig. 14. To anticipate saturation effects, the field distributions are analyzed for the flux density J = 1 T centric between the outer and inner ring diameter.

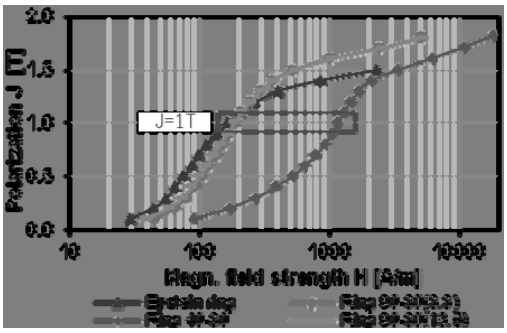

Fig. 14: The magnetization curves of the examined rings at 400 Hz.

The field distributions in a toroid inductor are radially symmetrical. Hence, it is sufficient to analyze the distribution of the flux density in the radial direction. As an example, the flux density distributions in the reference ring are illustrated in Fig. 15 (a) and (b). The origin of the axes lies in the center of the ring core. Due to the element size of 0.5 mm, the flux densities are sampled in the position y = ±0.25 mm and x = 135-165 mm. The sampled flux densities correspond to the magnetic field strengths, which relation is described by the measured magnetization curves.

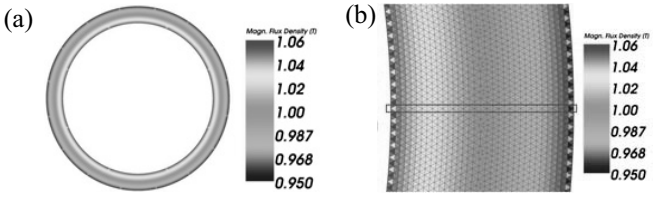

Fig. 15: (a) Field distribution in the reference ring and (b) detailed view.

The first ring to be examined is the reference ring core. In Fig. 16 can be seen, that due to the magnetic path length the highest flux densities are located at the inner diameter of the ring and vice versa. The flux density at the mean radius r_m = 150 mm are around 1 T, which serves as a reference value. The highest flux density at the inner radius of the ring r_i = 135 mm is J_{ri} = 1.056 T.

The corresponding magnetic field strength is H_{ri} = 188.25 A/m. The flux density at the mean radius of the ring is 1.005 T with a magnetic field strength of H_{rm} = 167.47 A/m. At the outer radius of the ring, the flux density reaches its minimum of J_{ra} = 0.962 T and corresponds to the magnetic field strength H_{ra} = 153.86 A/m. The relative deviation of the magnetic polarization can be calculated with the equation:

$$\frac{\Delta J_{r1-r2}}{J_{r2}} = \frac{J_{(r1)-(r2)}}{J_{r2}}. \qquad (6)$$

An analogous equation applies to the magnetic field strength. The relative deviation of the flux density and the field strength at the mean radius of the ring core is zero.

The flux density increases with smaller radius up to a value of 5.04 % higher than at the center r_m. At the outer radius, the minimum flux density is 4.25 % lower than at r_m. The absolute values of the flux density and its relative deviations from the center value J_{rm} of the reference ring as a function of the ring core radius are shown in Fig. 16. The difference of the polarizations at the inner and outer radius is $\Delta J_{ra-ri}/J_{ri}$ = 9.77%.

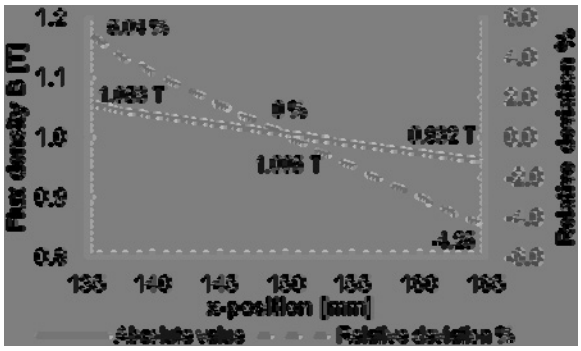

Fig. 16: The value and the relative deviation of the flux density in the reference ring.

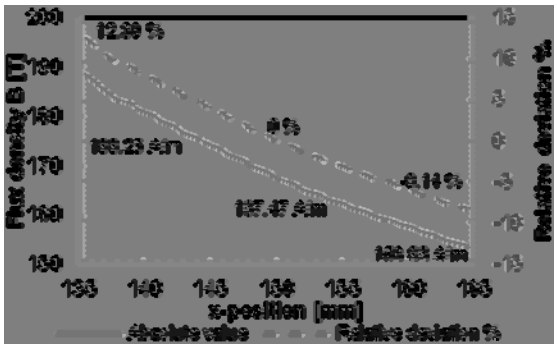

Fig. 17: The value and the relative deviation of the magnetic field strength in the reference ring.

In Fig. 17, the absolute values and the relative deviations of the corresponding magnetic field strength as a function of the ring core radius are presented. Due to the non-linearity of the magnetic properties, the relative deviations of the magnetic field strength are higher than the relative deviations of the flux density. The magnetic field strength at the inner radius of the ring core is 12.39 % higher than its reference value H_{rm}; at the outer radius, the value reaches its minimum with 8.14 % lower than H_{rm}. Moreover, one finds $\Delta H_{ra-ri} / H_{ri}$ = 22.35 %. The same simulation procedure is applied to the ring cores 90-30(3.3), 90-30(16.5), and 40-30. Due to the similarity of the magnetization curves of the rings 90-30 with the axial height of 3.3 mm and 16.5 mm (Fig. 14), the flux density distributions of both rings are also similar. Thus, it is sufficient to analyze the flux density distributions in one of the rings. The flux density distributions of the ring 90- 30(3.3) and 40-30 are illustrated in Fig. 18.

The difference of the polarization $\Delta J_{ra-ri}/J_{ri}$ and the field strength $\Delta H_{ra-ri}/H_{ri}$ at the outer and inner radius of each ring is analyzed. The reference ring has the lowest deviations of both values, with 9.77 % and 22.35 % respectively. The ring 40-30 of method 2 has deviations of $\Delta J_{ra-ri}/J_{ri}$ = 25.84 % and $\Delta H_{ra-ri}/H_{ri}$ = 30.41 %. The ring 90-30(3.3) and ring 90-30(16.5) has deviations of $\Delta J_{ra-ri}/J_{ri}$ = 110.29 % and

$\Delta H_{ra\text{-}ri}/H_{ri}$ = 230.95 %. These values are related to the ratio of the outer and inner diameter of the ring core. The reference ring, ring 40-30 of method 2, and ring 90-30 of method 1 and method 3 have the ratio d_o / d_i of 1.22, 1.33 and 3.00, respectively. The deviations increase with increasing d_o / d_i.

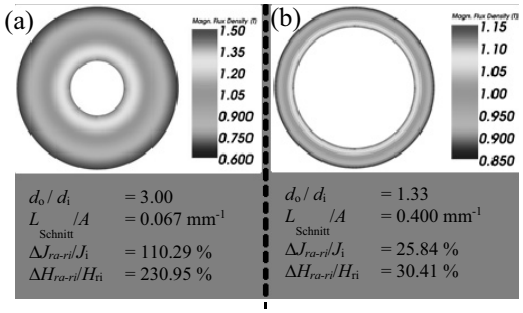

Fig. 18: Distribution of the flux densities inside the ring 90-30 (a) and the ring 40-30 (b).

IV. Numerical Simulation of a PMSM

In the next step, the measurement results of the magnetizing curves and the hysteresis losses are applied in 2D-FEM simulations of an existing PMSM using the smartFEM simulation tool. The utilized ring core measurement is chosen based on the stator geometry. The stator material of the PMSM is identical with the ring core material: electrical steel 280-30AP. The electrical steel M235-35A is used as rotor material. The geometry and the data of the PMSM is shown in Fig. 19.

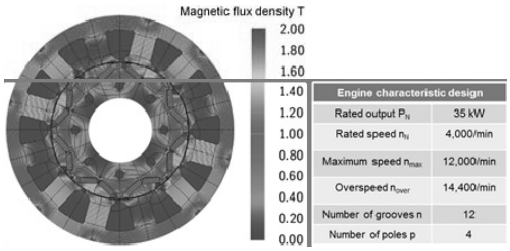

Fig. 19: Geometry and data of the PMSM.

The yoke width of the stator is 13 mm. Thus, the measurement results of the ring 60-40 of method 2 with a width in the radial direction of 10 mm is chosen, as it is the ring geometry which is closest to the yoke. In Fig. 20, the permeability curves of the Epstein strips and the ring core 60-40 are shown. To examine the influences of the characteristic curves of the used material in the simulation, the PMSM is simulated with both magnetization curves.

The simulations of the PMSM are performed for 2 operating points in base speed area with n_N = 4000 min^{-1}: OP 1 (nominal point) with $I_{str,N}$ = 85 A and OP 2 with I_{str} = 45 A. The machine has 4 pole pairs (p = 4) and an electrical frequency f = 266 Hz at n = 4000 min-1. The relation is:

$$f = \frac{n \cdot p}{60}. \quad (7)$$

Based on the simulation results with the magnetization curve from Epstein strips as material properties, the expected flux densities in the stator lie between 1.2 T and 1.5 T. For this reason, the measurement results between these points are analyzed. In the first step, the magnetization curves and the hysteresis losses will be studied. The influences of the material properties on the machine characteristics will be studied afterwards.

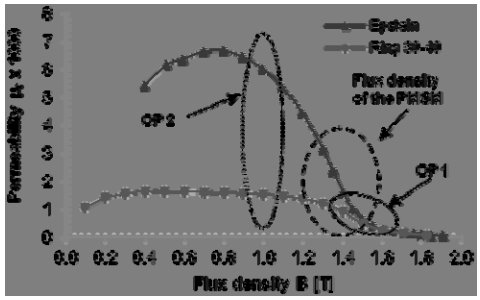

Fig. 20: Relative permeability of the Epstein strips and the ring core 60-40 at 50 Hz.

To compare the material characteristics, the magnetization curve and the hysteresis losses of the ring 60-40 are normalized to the measurement values of the Epstein procedure. In Fig. 21, the field strength factor of the ring 60-40 at 50 Hz is shown. The required magnetic fields to reach the polarizations of the ring 60-40 are generally higher than the field strengths required by the Epstein strips. The maximum difference is located at J = 0.8 T with the factor 4.15. The factor reaches its minimum at 1.6 T with the value of 1.15. Between 1.2 T and 1.5 T, which is expected in the stator, the values lie between 3.20 and 1.26.

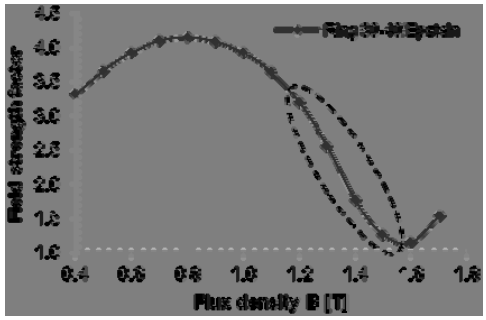

Fig. 21: Field strength factor of the ring 60-40 at 50 Hz.

Due to the electrical frequency of the PMSM at the simulated operating points, the hysteresis losses of the material parts are measured at 200 Hz and 400 Hz. The measurement results are presented in Fig. 22 as loss factors. Similar to the magnetization curves, the hysteresis losses of the ring 60-40 are generally higher than the losses of the Epstein strips. The hysteresis losses at 200 Hz and 400 Hz in the relevant area between 1.2 T and 1.5 T exhibit similar characteristics and values. Thus, it is not necessary to measure the parts at the PMSM operating point f = 266 Hz.

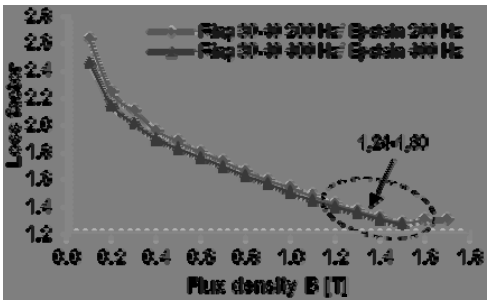

Fig. 22: Loss factor of the ring 60-40 at 200 Hz and 400 Hz.

The next step is to simulate the relevant operating points of the PMSM with the magnetization curve of the ring core 60-40. The simulation results are compared with the measurement results of the existing machine.
The simulated iron losses of the stator in the PMSM are shown in Fig. 23 (a). The difference in the magnetization curves of both parts leads to a change of the field distribution in the machine. The iron losses of the machine with the magnetizing curve of the ring core are higher than the simulated iron losses with the Epstein strips. In OP 1 (nominal point) the iron losses increase by 35.7 %, from 308 W to 418 W. In OP 2 (partial load) the iron losses increase by 46.1 %, from 191 to 279 W.

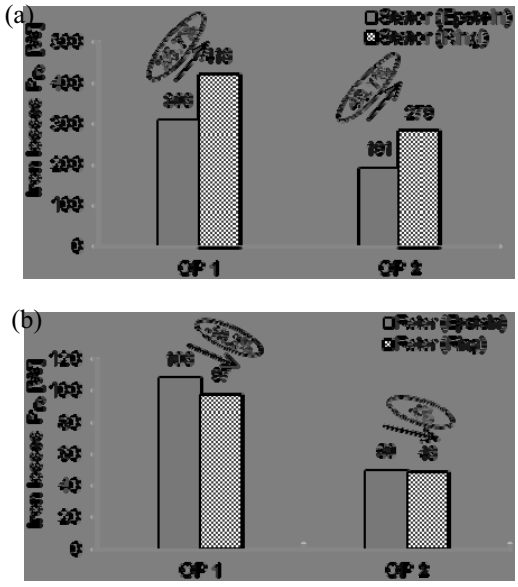

Fig. 23: Stator (a) and Rotor (b) iron losses of the PMSM, simulated with magnetizing curves of both parts.

Due to the lower magnetization of the stator through utilizing the ring core 60-40, the proportion of the rotating flux density decreases. This leads to decrease of iron losses. In the OP 1 and OP 2 the iron losses decrease by 10.2 % and 4 %, respectively, which is presented in Fig. 23 (b). The simulated and measured mechanical torque in the OP 1 (nominal point) are shown in Fig. 24. The value of the simulated output torque with the magnetization curves of the Epstein strips is 82.3 Nm. In the simulation utilizing the magnetization curve of the ring core 60-40, the torque drops by 1.94 % to 80.7 Nm. The measured output torque is 77.3 Nm, which is 6.08 % lower than the result of the simulation with the magnetization curve of the Epstein strips. The difference between the measured torque and the simulated torque with the magnetization curve of ring core 60-40 is 4.21 %. The simulation accuracy is slightly improved.

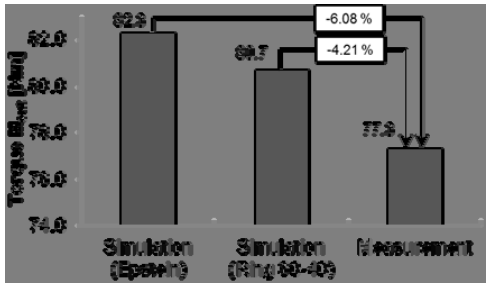

Fig. 24: The simulated and measured mechanical torque of the PMSM in OP 1 (nominal point).

The difference of the simulation results can be traced back to the relative permeability of both parts at the relevant flux densities, which is illustrated in Fig. 20.
The simulated and measured mechanical torque in OP 2 are shown in Fig 25. The simulated torque with the magnetizing curve of the Epstein strips is 41 Nm. Through utilizing the magnetizing curve of the ring core 60-40, the torque decreases by 2.68 % to 39.9 Nm. The measured torque is 39.6 Nm, which is very similar to the simulation results with the magnetizing curve of the ring core 60-40. Compared to the OP 1, the simulation accuracy is highly improved with 0.75 % deviation of the output torque.

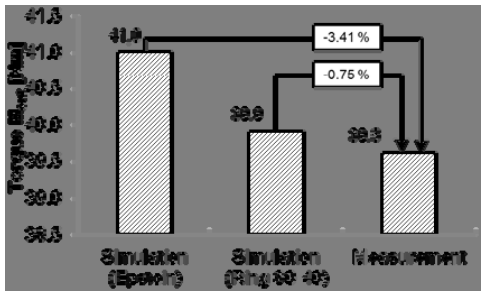

Fig. 25: Simulated and measured mechanical torque of the PMSM in OP 2.

The difference of the simulation results lies at the enormous difference of the relative permeability at J = 1 T, which is illustrated in Fig. 20.
The simulated and measured efficiency of the PMSM in OP 1 (nominal point) are shown in Fig. 26 (a). The application of the magnetizing curve of the ring core 60-40 leads to a drop of efficiency by 0.31 %, from 97.3 % to 96.99 %. However, the measured efficiency of the PMSM is 94.7 %.
The simulated and measured efficiency of the PMSM in OP 2 are presented in Fig. 26 (b). The decrease of the efficiency due to use of different magnetizing curves is slightly higher than in OP 1, by 0.51 %. The simulated efficiency with the magnetizing curve of the ring 60-40 is 97.19 %, which is 1.29 % higher than the measurement results.

(a)

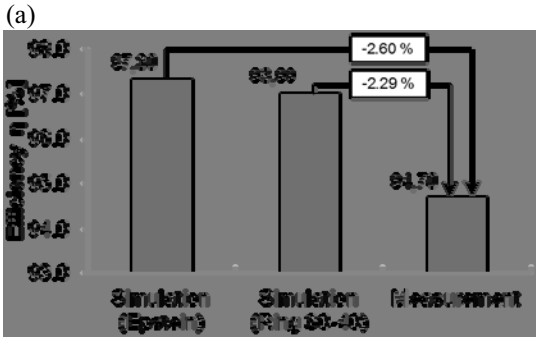

(b)

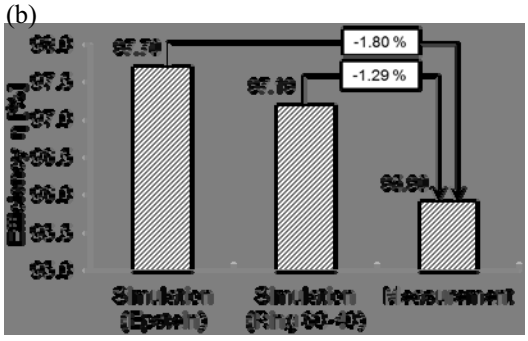

Fig. 26: Simulated and measured efficiency of the PMSM in OP 1 (a) (nominal point) and OP 2 (b).

V. Conclusion

In this manuscript, the experimental and numerical study of various ring core geometries are presented. The objective of the study is to describe the relationship of the geometry and the magnetic properties and the hysteresis losses of the samples. The measurement results serve as material properties in the simulation of electrical machines. Compared to the standardized Epstein strip, the ring core geometry has a better approximation to a stator geometry. Thus, the measured magnetic properties of the ring core are more similar to the stator of electrical machines. The norm IEC 60404-6 specifies the requirement of a ring core geometry (d_o / d_i < 1.4, preferably d_o / d_i < 1.25) used for measurements of magnetic properties, which is taken into account in the performed study.
Three methods to modify the ring core geometry are studied. The results are compared with a reference ring, with a magnetic path length identical to the path length in an Epstein frame. It can be concluded, that the axial height of the ring core does not have any crucial effect on the magnetic properties of the ring core. On the contrary, the ratio of outer to inner diameter of the ring core do / di and the ratio of cutting edge length to the ring core area L_{cut}/A have huge influences on the magnetic properties. 2D numerical examinations are performed to evaluate the field distribution in the ring cores. The shifting of the magnetizing curves due to the axial height is analogous to an electrical machine with different axial length. Here, it is shown, that the ratio of the diameters strongly influences the flux density distributions.
A PMSM is simulated with measured magnetizing curves of Epstein strips and a ring core. In the stator, one finds higher iron losses in OP1 as well as in OP2 of about 36% and 46%, respectively, for the simulation based on the ring core data. In contrast, in the rotor, the losses are lower, i.e. 10% in OP1 and 4% in OP2. Nevertheless, the total losses of the machine are still higher in case of using ring core data for the simulation.
Due to the magnetizing curves, the simulated mechanical torques decrease by 2 % in OP 1 (nominal point) and 2.68 % in OP 2 (partial load). The measured mechanical torques at OP 1 and OP 2 are 6.08 % and 3.41 % lower than the mechanical torques from the first simulations. The simulated efficiencies decrease by 0.31 % in OP 1, from 97.3 % to 96.99 %. In OP 2, the simulated efficiencies sink by 0.51 %, from 97.7 % to 96.99 %. The measured efficiencies at OP 1 and OP 2 are 94.7 % and 95.9%, respectively.
Using the magnetizing curve of the ring core, the simulation accuracy can be improved. However, this method only applies to electrical machines. For further improvement of the simulation accuracy, additional methods are required. The stator yoke and teeth, which can be represented by ring core and Epstein strips respectively, have to be considered separately. In addition, the 3-phaseconverter, which feeds the machine, induces nonsinusoidal signals. This leads to development of higher harmonics in the flux density distributions and has to be taken into account for the characterization of the magnetic properties.

Acknowledgment

The authors would like to thank G. Padalikar for samples preparation. Further thanks are due to B. Runge for fruitful discussions.

Reference

[1] Schoppa, A.P.: Einfluss der Be- und Verarbeitung auf die magnetischen Eigenschaften von schlussgeglühtem, nichtkornorientiertem Elektroband Rheinisch Westfälischen Technische Hochschule Aachen, Dissertation, 2001.
[2] IEC 60404-2: Magnetic materials - Part 2: Methods of measurement of the magnetic properties of electrical steel strip and sheet by means of an Epstein frame, 2009.
[3] IEC 60404-6: Magnetic materials - Part 6: Methods of measurement of the magnetic properties of magnetically soft metallic and powder materials at frequencies in the range of 20 Hz to 200 kHz by the use of ring specimens, 2004.
[4] DIN 50460:1986-09: Bestimmung der magnetischen Eigenschaften von weichmagnetischen Werkstoffen; Allgemeines, Begriffe, Grundlagen der Prüfverfahren.